
Descent Steps of a Relation-Aware Energy Produce Heterogeneous Graph Neural Networks

Hongjoon Ahn^{1*}, Yongyi Yang^{2*}, Quan Gan³, Taesup Moon¹ and David Wipf³

¹ Seoul National University, ² Fudan University, ³ Amazon Web Services,
{hong0805, tsmoon}@snu.ac.kr,
yongyiyang17@fudan.edu.cn,
quagan@amazon.com,
davidwipf@gmail.com

Abstract

Heterogeneous graph neural networks (GNNs) achieve strong performance on node classification tasks in a semi-supervised learning setting. However, as in the simpler homogeneous GNN case, message-passing-based heterogeneous GNNs may struggle to balance between resisting the oversmoothing occurring in deep models and capturing long-range dependencies graph structured data. Moreover, the complexity of this trade-off is compounded in the heterogeneous graph case due to the disparate heterophily relationships between nodes of different types. To address these issues, we proposed a novel heterogeneous GNN architecture in which layers are derived from optimization steps that descend a novel relation-aware energy function. The corresponding minimizer is fully differentiable with respect to the energy function parameters, such that bilevel optimization can be applied to effectively learn a functional form whose minimum provides optimal node representations for subsequent classification tasks. In particular, this methodology allows us to model diverse heterophily relationships between different node types while avoiding oversmoothing effects. Experimental results on 8 heterogeneous graph benchmarks demonstrates that our proposed method can achieve competitive node classification accuracy.

1 Introduction

Graph structured data, which contains information related to entities as well as the interactions between them, arise in various applications such as social networks or movie recommendations. In a real world scenario, these entities and interactions are often multi-typed (*e.g.*, actor, director, keyword, and movie in a movie review graph[19] or authors, papers, terms, and venue in an academic network [30]), and hence the relationships between entities can potentially become much more complex than a homogeneous graph scenario, in which only a single node and edge type exists. To this end, *heterogeneous* graphs have been proposed as a practical and effective tool to systematically deal with such multi-typed graph-structured data. With the advent of graph neural networks (GNN) for instantiating deep models that are sensitive to complex relationships between data instances, it is natural that multiple variants have been developed to explicitly handle heterogeneous graphs [4, 6, 10, 32, 28, 17], with promising performance on downstream tasks such as node classification or link prediction.

In this vein, message-passing GNNs represent one of the most widely-adopted heterogeneous architectures, whereby a sequence of type-specific graph propagation operators allow neighboring nodes

*Work completed during an internship at the AWS Shanghai AI Lab.

to share and aggregate heterogeneous information [6, 28, 32]. However, in some cases where long-range dependencies exist between nodes across the graph, stacking too many layers to reflect a larger neighborhood may contribute to a well-known *oversmoothing* problem, in which node features converge to similar, non-discriminative embeddings [16, 21]. In the case of homogeneous graphs, this oversmoothing problem has been addressed (among other methods) using modified GNN architectures with layers patterned after the unfolded descent steps of some graph-regularized energy [7, 34]. Provided minimizers of this energy remain discriminative for the task at hand, arbitrarily deep networks can be trained without risk of oversmoothing, with skip connections between layers organically emerging to favor node-specific embeddings. However, extending this approach to handle heterogeneous graphs is not straightforward, largely because node/edge heterogeneity (*e.g.*, node-specific numbers of classes or feature dimensions, multiple types of relationships between nodes) is not easily reflected in the vanilla energy functions adopted thus far for the homogeneous graphs. In particular, existing energy functions are mostly predicated on the assumption of graph homophily, whereby neighboring nodes have similar labels. But in the heterogeneous case this assumption is no longer realistic because the labels between nodes of different types may exhibit complex relationships.

To this end, we first introduce a novel heterogeneous GNN architecture with layers produced by the minimization of a relation-aware energy function. This energy produces regularized heterogeneous node embeddings, relying on relation-dependent compatibility matrices as have been previously adopted in the context of belief propagation on heterogeneous graphs, *e.g.*, ZooBP [5]. Secondly, we derive explicit propagation rules for our model layers by computing gradient descent steps along the proposed energy, with quantifiable convergence conditions related to the learning rate considered as well. Furthermore, we provide interpretations of each component of the resulting propagation rule, which consists of skip-connections, linearly transformed feature aggregation, and a self-loop transformation. With respect to experiments, our contributions are twofold. First, we show that our algorithm outperforms state-of-the-art baselines on various benchmark datasets. And secondly, we analyze the effectiveness of using the compatibility matrix and the behavior of the unfolding step as the number of propagations increases.

2 Existing Homogeneous GNNs from Unfolded Optimization

Consider a *homogeneous* graph $\mathcal{G} = \{\mathcal{V}, \mathcal{E}\}$, with $n = |\mathcal{V}|$ nodes and $m = |\mathcal{E}|$ edges. We define $\mathbf{L} \in \mathbb{R}^{n \times n}$ as the Laplacian of \mathcal{G} , meaning $\mathbf{L} = \mathbf{D} - \mathbf{A}$, in which \mathbf{D} and \mathbf{A} are degree and adjacency matrices, respectively. Unfolded GNNs incorporate graph structure by attaining optimized embeddings $\mathbf{Y}^* \in \mathbb{R}^{n \times d}$ that are functions of some adjustable weights \mathbf{W} , *i.e.*, $\mathbf{Y}^* \equiv \mathbf{Y}^*(\mathbf{W})$ ², where $\partial \mathbf{Y}^*(\mathbf{W}) / \partial \mathbf{W}$ is computable by design. Then, these embeddings are inserted within an application-specific loss

$$\ell_{\boldsymbol{\theta}}(\boldsymbol{\theta}, \mathbf{W}) \triangleq \sum_{i=1}^{n'} \mathcal{D}(g[\mathbf{y}_i^*(\mathbf{W}); \boldsymbol{\theta}], \mathbf{t}_i), \quad (1)$$

in which $g : \mathbb{R}^d \rightarrow \mathbb{R}^c$ is some differentiable node-wise function with parameters $\boldsymbol{\theta}$ and c -dimensional output tasked with predicting ground-truth node-wise targets $\mathbf{t}_i \in \mathbb{R}^c$. Additionally, $\mathbf{y}_i^*(\mathbf{W})$ is the i -th row of $\mathbf{Y}^*(\mathbf{W})$, $n' < n$ is the number of labeled nodes (we assume *w.l.o.g.* that the first n' nodes are labeled), and \mathcal{D} is a discriminator function, *e.g.*, cross-entropy for node classification, as will be our focus. Given that $\mathbf{Y}^*(\mathbf{W})$ is differentiable by construction, we can optimize $\ell_{\boldsymbol{\theta}}(\boldsymbol{\theta}, \mathbf{W})$ via gradient descent (over both $\boldsymbol{\theta}$ and \mathbf{W} if desired) to obtain our final predictive model.

At a conceptual level, what differentiates GNNs inspired by unfolded optimization is how $\mathbf{Y}^*(\mathbf{W})$ is obtained. Specifically, these node embeddings are chosen to be the minimum of a lower-level, graph-regularized energy function [2, 18, 22, 34, 35, 37]. Originally inspired by [36], the most common selection for this energy is given by

$$\ell_{\mathcal{Y}}(\mathbf{Y}; \mathbf{W}) \triangleq \|\mathbf{Y} - f(\mathbf{X}; \mathbf{W})\|_{\mathcal{F}}^2 + \lambda \text{tr}[\mathbf{Y}^{\top} \mathbf{L} \mathbf{Y}], \quad (2)$$

where $\lambda > 0$ is a trade-off parameter, $\mathbf{Y} \in \mathbb{R}^{n \times d}$ is a matrix of trainable embeddings, meaning d -dimensional features across n nodes, and $f(\mathbf{X}; \mathbf{W})$ is a base model parameterized by \mathbf{W} that produces initial target embeddings using the d_0 -dimensional node features $\mathbf{X} \in \mathbb{R}^{n \times d_0}$.

²For brevity, we will frequently omit this dependency on \mathbf{W} when the context is clear.

Minimization of (2) over \mathbf{Y} results in new node embeddings \mathbf{Y}^* characterized by a balance between similarity with $f(\mathbf{X}; \mathbf{W})$ and smoothness across graph edges as favored by the trace term $\text{tr}[\mathbf{Y}^\top \mathbf{L} \mathbf{Y}] = \sum_{\{i,j\} \in \mathcal{E}} \|\mathbf{y}_i - \mathbf{y}_j\|_2^2$, where \mathbf{y}_i is i -th row of \mathbf{Y} . While (2) can be solved in a closed-form as

$$\mathbf{Y}^*(\mathbf{W}) = \arg \min_{\mathbf{Y}} \ell_y(\mathbf{Y}; \mathbf{W}) = (\mathbf{I} + \lambda \mathbf{L})^{-1} f(\mathbf{Y}; \mathbf{W}), \quad (3)$$

for large graphs this analytical solution is not practically computable. Instead, we may form initial node embeddings $\mathbf{Y}^{(0)} = f(\mathbf{X}; \mathbf{W})$, and then apply gradient descent to converge towards the minimum, with the k -th iteration given by

$$\mathbf{Y}^{(k)} = \mathbf{Y}^{(k-1)} - \alpha \left[(\lambda \mathbf{L} + \mathbf{I}) \mathbf{Y}^{(k-1)} - f(\mathbf{X}; \mathbf{W}) \right], \quad (4)$$

in which $\frac{\alpha}{2}$ is the step size. Given that \mathbf{L} is generally sparse, computation of (4) can leverage efficient sparse matrix multiplications. Combined with the fact that the loss is strongly convex, and provided that α is chosen suitably small, we are then guaranteed to converge towards the unique global optima with efficient gradient steps, meaning that for some K sufficiently large $\mathbf{Y}^{(K)}(\mathbf{W}) \approx \mathbf{Y}^*(\mathbf{W})$.

Critically, $\mathbf{Y}^{(K)}(\mathbf{W})$ remains differentiable with respect to \mathbf{W} , such that we may substitute this value into (1) in place of $\mathbf{Y}^*(\mathbf{W})$ to obtain an entire pipeline that is end-to-end differentiable w.r.t. \mathbf{W} . Moreover, per the analyses from [18, 22, 34, 35, 37], the k -th *unfolded* iteration of (4) can be interpreted as an efficient form of GNN layer. In fact, for certain choices of the step size, and with the incorporation of gradient pre-conditioning and other reparameterization factors, these iterations can be exactly reduced to popular canonical GNN layers such as those used by GCN [14], APPNP [7], and others. However, under broader settings, we obtain unique GNN layers that are naturally immune to oversmoothing, while nonetheless facilitating long-range signal propagation across the graph by virtue of the anchoring effect of the underlying energy function. In other words, regardless of how large K is, these iterations/layers will converge to node embeddings that adhere to the design criteria of (2). This is the distinct appeal of GNN layers motivated by unfolded optimization, at least thus far in the case of homogeneous graphs.

3 New Heterogeneous GNN Layers via Unfolding

In this section, we explore novel extensions of unfolded optimization to handle heterogeneous graphs, which, as mentioned previously, are commonly encountered in numerous practical application domains. After introducing our adopted notation, we first describe two relatively simple, intuitive attempts to accommodate heterogeneous node and edge types. We then point out the shortcomings of these models, which are subsequently addressed by our main proposal: a general-purpose energy function and attendant proximal gradient steps that both (i) descend the aforementioned energy, and (ii) in doing so facilitate flexible node- and edge-type dependent message passing with non-linear activations where needed. The result is a complete, interpretable heterogeneous GNN (HGNN) architecture with layers in one-to-one correspondence with the minimization of a heterogeneous graph-regularized energy function.

Before we begin, we introduce some additional notation. An undirected heterogeneous graph $\mathcal{G} = (\mathcal{V}, \mathcal{E})$ is a collection of node types \mathcal{S} and edge types \mathcal{T} such that $\mathcal{V} = \bigcup_{s \in \mathcal{S}} \mathcal{V}_s$ and $\mathcal{E} = \bigcup_{t \in \mathcal{T}} \mathcal{E}_t$. Here \mathcal{V}_s denotes a set of $n_s = |\mathcal{V}_s|$ nodes of type s , while \mathcal{E}_t represents a set of edge type t . Furthermore, we use $\mathcal{T}_{ss'}$ to refer to the set of edge types connecting node types s and s' . Note that \mathcal{T} includes both the canonical direction, $t \in \mathcal{T}_{ss'}$, and the inverse direction, $t_{\text{inv}} \in \mathcal{T}_{s's}$, that corresponds with a type t edge.³

3.1 First Attempts at Heterogeneous Unfolding

A natural starting point for extending existing homogeneous models to the heterogeneous case would be to adopt the modified energy

$$\ell_{\mathbf{Y}}(\mathbf{Y}) \triangleq \sum_{s \in \mathcal{S}} \left[\frac{1}{2} \|\mathbf{Y}_s - f(\mathbf{X}_s; \mathbf{W}_s)\|_{\mathcal{F}}^2 + \frac{\lambda}{2} \sum_{s' \in \mathcal{S}} \sum_{t \in \mathcal{T}_{ss'}} \text{tr}(\mathbf{Y}^\top \mathbf{L}_t \mathbf{Y}) \right], \quad (5)$$

in which \mathbf{L}_t is the graph Laplacian involving all edges of relation type t and \mathbf{W}_s parameterizes a type-specific transformation of node representations. Here, we have simply introduced type-specific

³For example, if $t \in \mathcal{T}_{ss'}$ is ("paper"- "author"), then $t_{\text{inv}} \in \mathcal{T}_{s's}$ is ("author"- "paper")

transformations of the initial node representations, as well as adding a separate graph regularization term for each relation type t . However, this formulation is actually quite limited as it can be reduced to the equivalent energy

$$\ell_{\mathbf{Y}}(\mathbf{Y}) \equiv \frac{1}{2} \left\| \mathbf{Y} - \tilde{f}(\tilde{\mathbf{X}}; \mathcal{W}) \right\|_{\mathcal{F}}^2 + \frac{\lambda}{2} \text{tr}(\mathbf{Y}^{\top} \mathbf{C} \mathbf{Y}), \quad \text{with } \mathbf{C} = \sum_{s \in \mathcal{S}} \sum_{s' \in \mathcal{S}} \sum_{t \in \mathcal{T}_{ss'}} \mathbf{L}_t, \quad (6)$$

in which $\tilde{\mathbf{X}}$ represents the original node features concatenated with the node type, and \tilde{f} is some function of the augmented features parameterized by $\mathcal{W} \triangleq \{\mathbf{W}_s\}_{s \in \mathcal{S}}$. Note that by construction, \mathbf{C} will necessarily be positive semi-definite, and hence we may then conclude through (6) that (5) defaults to the form of a standard quadratically-regularized loss, analogous to (2), that has often been applied to graph signal processing problems [12]. Therefore the gradient descent iterations of this objective will closely mirror the existing homogeneous unfolded GNN architectures described in Section 2, and fail to capture the nuances of heterogeneous data.

To break the symmetry that collapses all relation-specific regularization factors into $\text{tr}(\mathbf{Y}^{\top} \mathbf{C} \mathbf{Y})$, a natural option is to introduce t -dependent weights as in

$$\ell_{\mathbf{Y}}(\mathbf{Y}) \triangleq \sum_{s \in \mathcal{S}} \left[\frac{1}{2} \left\| \mathbf{Y}_s - f(\mathbf{X}_s; \mathbf{W}_s) \right\|_{\mathcal{F}}^2 + \frac{\lambda}{2} \sum_{s' \in \mathcal{S}} \sum_{t \in \mathcal{T}_{ss'}} \text{tr}(\mathbf{Y}^{\top} \mathbf{L}_t \mathbf{Y} \mathbf{M}_t) \right], \quad (7)$$

in which the set $\{\mathbf{M}_t\}$ is trainable. While certainly more expressive than (5), this revision is nonetheless saddled with several key limitations: (i) Unless additional constraints are included on $\{\mathbf{M}_t\}$ (e.g., PSD, etc.), (7) may be unbounded from below; (ii) While \mathbf{M}_t may be asymmetric, w.l.o.g. the loss can be equivalently expressed with symmetric weights, and hence the true degrees of freedom are limited; (iii) This model could be prone to overfitting, since during training it could be that $\mathbf{M}_t \rightarrow 0$ in which case the graph-based regularization is turned off;⁴ and (iv) because $\text{tr}[\mathbf{Y}^{\top} \mathbf{L}_t \mathbf{Y} \mathbf{M}_t] = \sum_{(i,j) \in \mathcal{E}_t} (\mathbf{y}_i - \mathbf{y}_j)^{\top} \mathbf{M}_t (\mathbf{y}_i - \mathbf{y}_j)$, the energy function (7) is symmetric w.r.t. the order of the nodes in the regularization term, and therefore any derived message passing must also be symmetric, *i.e.*, we cannot exploit asymmetric penalization aligned with heterogeneous relationships in the data.

Given then that both (5) and (7) have notable shortcomings, it behooves us to consider revised criteria for selecting a suitable heterogeneous energy function. We explore such issues next.

3.2 A More Expressive Alternative Energy Function

As an entry point for developing a more flexible class of energy functions that is sensitive to nuanced relationships between different node types, we consider previous work developing various flavors of both label and belief propagation [5, 26, 33, 36]. In the more straightforward setting of homogeneous graphs under homophily conditions, label propagation serves as a simple iterative process for smoothing known training labels across edges to unlabeled nodes in such a way that, for a given node i , the predicted node label $\hat{\mathbf{t}}_i$ will approximately match the labels of neighboring nodes \mathcal{N}_i , *i.e.*, $\hat{\mathbf{t}}_i \approx \hat{\mathbf{t}}_j$ when $j \in \mathcal{N}_i$; an analogous relationship holds when labels are replaced with beliefs [26].

However, in broader regimes with varying degrees of heterophily, it is no longer reasonable for such a simple relationship to hold, as neighboring nodes may be more inclined to have *dissimilar* labels. To address this mismatch, a compatibility matrix \mathbf{H} must be introduced such that now label propagation serves to instantiate $\hat{\mathbf{t}}_i \approx \hat{\mathbf{t}}_j \mathbf{H}$ for $j \in \mathcal{N}_i$ [33] (here we treat each $\hat{\mathbf{t}}_j$ as a row vector). If each predicted label $\hat{\mathbf{t}}_i$ is approximately a one-hot vector associated with class membership probabilities, then the (k, l) -th element of \mathbf{H} roughly determines how a node of class k influences neighbors of class l . And if we further extend to heterogeneous graphs as has been done with various forms of belief propagation [5], it is natural to maintain a unique (possibly non-square) compatibility matrix \mathbf{H}_t for each relation type t , with the goal of finding predicted labels (or beliefs) of each node type satisfying $\hat{\mathbf{t}}_{si} \approx \hat{\mathbf{t}}_{s'j} \mathbf{H}_t$ for $s, s' \in \mathcal{S}$, $t \in \mathcal{T}_{ss'}$, and $(i, j) \in \mathcal{E}_t$. From a practical standpoint, each

⁴For example, suppose the node features of training nodes are highly correlated with the labels, or actually are the labels (as in some prior label propagation work). Then the model could just learn $\mathbf{M}_t = 0$ and achieve perfect reconstruction on the training nodes to produce zero energy, and yet overfit since graph propagation is effectively turned off.

such \mathbf{H}_t can be estimated from the data using the statistics of the labels (or beliefs) of nodes sharing edges of type t .

Returning to our original goal, we can use similar intuitions to guide the design of an appropriate regularization factor for learning heterogeneous graph node representations (as required by HGNNs). Specifically, given $s, s' \in \mathcal{S}$, $t \in \mathcal{T}_{ss'}$, and $(i, j) \in \mathcal{E}_t$, we seek to enforce $\mathbf{y}_{si}\mathbf{H}_t \approx \mathbf{y}_{s'j}$, which then naturally motivates the energy

$$\ell_{\mathbf{Y}}(\mathbf{Y}) \triangleq \sum_{s \in \mathcal{S}} \left[\frac{1}{2} \|\mathbf{Y}_s - f(\mathbf{X}_s; \mathbf{W}_s)\|_{\mathcal{F}}^2 + \frac{\lambda}{2} \sum_{s' \in \mathcal{S}} \sum_{t \in \mathcal{T}_{ss'}} \sum_{(i,j) \in \mathcal{E}_t} \|\mathbf{y}_{si}\mathbf{H}_t - \mathbf{y}_{s'j}\|_2^2 \right], \quad (8)$$

where λ denotes a trade-off parameter, $\mathbf{X}_s \in \mathbb{R}^{n_s \times d_{0s}}$ is d_{0s} -dimensional initial features and $\mathbf{Y}_s \in \mathbb{R}^{n_s \times d_s}$ represents the embedding of d_s -dimensional features on n_s nodes for node type s . Note that \mathbf{y}_{si} and $\mathbf{y}_{s'j}$ are the i -th and j -th row of \mathbf{Y}_s and $\mathbf{Y}_{s'}$, respectively. Additionally, $\mathbf{H}_t \in \mathbb{R}^{d_s \times d_{s'}}$ denotes a compatibility matrix that matches the dimension of two different node embeddings (*i.e.*, \mathbf{y}_i and \mathbf{y}_j) via linear transformation for edge type t .

The energy function (8) exhibits the following two characteristics:

- The first term prefers that the embedding \mathbf{Y}_s should be close to that from $f(\mathbf{X}_s; \mathbf{W}_s)$.
- The second term prefers that for two connected nodes of type s and s' , the embeddings $\mathbf{y}_{si}\mathbf{H}_t$ and $\mathbf{y}_{s'j}$ should be relatively close to one another.

Even when the dimensions of two embeddings are the same (*i.e.*, $d_s = d_{s'}$), \mathbf{H}_t still serves an important role in allowing the embeddings to lie within different subspaces to obtain compatibility.

3.3 Analysis and Derivation of Corresponding Descent Steps

The objective (8) can be written as a matrix form as follows:

$$\ell_{\mathbf{Y}}(\mathbf{Y}) = \sum_{s \in \mathcal{S}} \left[\frac{1}{2} \|\mathbf{Y}_s - f(\mathbf{X}_s; \mathbf{W}_s)\|_{\mathcal{F}}^2 + \frac{\lambda}{2} \sum_{s' \in \mathcal{S}} \sum_{t \in \mathcal{T}_{ss'}} \left[\text{tr}((\mathbf{Y}_s \mathbf{H}_t)^\top \mathbf{D}_{st} (\mathbf{Y}_s \mathbf{H}_t) - 2(\mathbf{Y}_s \mathbf{H}_t)^\top \mathbf{A}_t \mathbf{Y}_{s'} + \mathbf{Y}_{s'}^\top \mathbf{D}_{s't_{\text{inv}}} \mathbf{Y}_{s'}) \right] \right], \quad (9)$$

where \mathbf{A}_t denotes the adjacency matrix for an edge type t , and \mathbf{D}_{st} denotes the type- t degree matrix of type- s nodes.

The closed-form optimal point of (9) is provided by the following results; see the Supplementary Materials for the proof.

Lemma 3.1. *The closed-form solution minimizing (9) is as follows:*

$$\text{vec}(\mathbf{Y}^*(\mathcal{W}, \mathcal{H})) = (\mathbf{I} + \lambda(\mathbf{Q} - \mathbf{P} + \mathbf{D}))^{-1} \text{vec}(\tilde{f}(\tilde{\mathbf{X}}; \mathcal{W})), \quad (10)$$

where $\text{vec}(\mathbf{B}) = [\mathbf{b}_1^\top, \dots, \mathbf{b}_n^\top]^\top$ for matrix \mathbf{B} , $\mathcal{H} \triangleq \{\mathbf{H}_t\}_{t \in \mathcal{T}}$ denotes a set for all compatibility matrices, and we define the matrices \mathbf{P} , \mathbf{Q} , and \mathbf{D} as

$$\mathbf{P} = \begin{bmatrix} \mathbf{P}_{11} & \dots & \mathbf{P}_{1|\mathcal{S}|} \\ \dots & \dots & \dots \\ \mathbf{P}_{|\mathcal{S}|1} & \dots & \mathbf{P}_{|\mathcal{S}||\mathcal{S}|} \end{bmatrix}; \mathbf{P}_{ss'} = \sum_{t \in \mathcal{T}_{ss'}} ((\mathbf{H}_t^\top + \mathbf{H}_{t_{\text{inv}}}) \otimes \mathbf{A}_t)$$

$$\mathbf{Q} = \bigoplus_{s \in \mathcal{S}} \mathbf{Q}_s; \mathbf{Q}_s = \sum_{s' \in \mathcal{S}} \sum_{t \in \mathcal{T}_{ss'}} (\mathbf{H}_t \mathbf{H}_t^\top \otimes \mathbf{D}_{st}), \mathbf{D} = \bigoplus_{s \in \mathcal{S}} \mathbf{I} \otimes \mathbf{D}_s.$$

Here \otimes denotes the Kronecker product, $\bigoplus_{i=1}^n \mathbf{A}_i = \text{diag}(\mathbf{A}_1, \dots, \mathbf{A}_n)$ denotes a direct sum of n square matrices $\mathbf{A}_1, \dots, \mathbf{A}_n$, and $\mathbf{D}_s \triangleq \sum_{s' \in \mathcal{S}} \sum_{t \in \mathcal{T}_{ss'}} \mathbf{D}_{s't}$ represent a sum of degree matrices over all node types $s' \in \mathcal{S}$ and all edge types $t \in \mathcal{T}_{ss'}$.

We can interpret this solution as transforming $\tilde{f}(\tilde{\mathbf{X}}; \mathcal{W})$ into an embedding that has both local and global information of the graph structure [36]. Therefore, this can be treated as an appropriate graph-aware embedding for carrying out a downstream task such as node classification.

However, for large graph data, computing the inverse, $(\mathbf{I} + \lambda(\mathbf{Q} - \mathbf{P} + \mathbf{D}))^{-1}$, in (24) is extremely expensive. To resolve this issue, similar to the homogeneous case we instead apply gradient descent to (9) over \mathbf{Y}_s for all node type $s \in \mathcal{S}$ to approximate $\mathbf{Y}^*(\mathcal{W}, \mathcal{H})$. Starting from the initial point $\mathbf{Y}_s^{(0)} = f(\mathbf{X}_s; \mathbf{W}_s)$ for each $s \in \mathcal{S}$, several steps of gradient descent are performed to obtain an appropriate embedding for carrying out a downstream task. Since all the intermediate steps of gradient descent are differentiable features w.r.t \mathcal{W} and \mathcal{H} , we can just plug-in the result of performing K iterations of gradient descent, $\mathbf{Y}_s^{(K)}$, into the (18).

In order to get $\mathbf{Y}_s^{(K)}$ using gradient descent, we first compute the gradient of (9) w.r.t \mathbf{Y}_s ;

$$\nabla_{\mathbf{Y}_s} \ell_{\mathbf{Y}}(\mathbf{Y}) = (\mathbf{I} + \lambda \mathbf{D}_s) \mathbf{Y}_s - f(\mathbf{X}_s; \mathbf{W}_s) + \lambda \sum_{s' \in \mathcal{S}} \sum_{t \in \mathcal{T}_{ss'}} (\mathbf{D}_{st} \mathbf{Y}_s (\mathbf{H}_t \mathbf{H}_t^\top) - \mathbf{A}_t \mathbf{Y}_{s'} (\mathbf{H}_t^\top + \mathbf{H}_{t_{\text{inv}}})) \quad (11)$$

Note, if the condition number of (20) is large, the convergence speed of gradient descent can be slow [20]. To reduce the convergence time effectively, we use the Jacobi preconditioning technique [1] that rescales the gradient step using $\tilde{\mathbf{D}}_s^{-1} \triangleq (\mathbf{I} + \lambda \mathbf{D}_s)^{-1}$. Then, the iteration $k + 1$ of gradient descent on \mathbf{Y}_s can be computed as

$$\mathbf{Y}_s^{(k+1)} = \underbrace{(1 - \alpha) \mathbf{Y}_s^{(k)}}_{(a)} + \alpha \tilde{\mathbf{D}}_s^{-1} \left[\underbrace{f(\mathbf{X}_s; \mathbf{W}_s)}_{(b)} + \lambda \sum_{s' \in \mathcal{S}} \sum_{t \in \mathcal{T}_{ss'}} \left(\underbrace{\mathbf{A}_t \mathbf{Y}_{s'}^{(k)} (\mathbf{H}_t^\top + \mathbf{H}_{t_{\text{inv}}})}_{(c)} - \underbrace{\mathbf{D}_{st} \mathbf{Y}_s^{(k)} (\mathbf{H}_t \mathbf{H}_t^\top)}_{(d)} \right) \right], \quad (12)$$

where α denotes a step size. The above expression can be considered as a forward propagation rule for the k -th layer in a GNN model. In (25), the terms (a), (b), (c), and (d) can be interpreted as follows:

Terms (a) & (b) Each term can be treated as a skip connection from the previous layer $\mathbf{Y}_s^{(k)}$ and the input features $f(\mathbf{X}_s; \mathbf{W}_s)$, respectively. Unlike some previous work [15, 17] that adopted skip-connections as a heuristic solution to resolve the oversmoothing problem [16, 21], similar to the unfolded GNN in homogeneous case [34, 7], the skip connections in our expression are naturally derived from the gradient descent step for minimizing the energy function.

Term (c) This term accumulates the propagated feature vectors of neighboring nodes. The matrix $\mathbf{H}_t^\top + \mathbf{H}_{t_{\text{inv}}}$ serves as edge-type specific transformations in a bi-directional way. Note that all matrices in \mathcal{H} are shared across all propagation layers, and as a result, the number of parameters does not increase as the propagation proceeds.

Term (d) This term is a self-loop transformation that depends on the edge type t . The matrix $\mathbf{H}_t \mathbf{H}_t^\top$ introduces an edge-type specific transformation in a uni-directional way, and the matrix \mathbf{D}_{st} reflects the strength of the self-loop transformation relying on edge type t . Note that, unlike prior work [17, 28], we use edge-type specific degree and transformation matrices, and these are also shared across all GNN layers.

We reiterate that all components of (25) have naturally emerged from the gradient descent procedure for minimizing the underlying energy function. And in terms of convergence, we address how executing the stated unfolding steps with an appropriate α produces a global minimum of (9), $\mathbf{Y}^*(\mathcal{W}, \mathcal{H})$. (Note that if we choose a relatively large α the energy function value may diverge such that the graph structure is not properly reflected.) To this end, we have the following, with the proof deferred to the Supplementary Materials.

Theorem 3.2. *A sufficient condition for convergence of the iteration from (25) is that α satisfies*

$$\alpha < \frac{2 + 2\lambda d_{\min}}{1 + \lambda(d_{\min} + \sigma_{\max})}, \quad (13)$$

where $d_{\min} \triangleq \min_i \mathbf{D}_{ii}$ is the minimum degree, and σ_{\max} is a maximum eigenvalue of matrix $(\mathbf{Q} - \mathbf{P})$.

Time Complexity Although seemingly complicated, the time complexity of executing (25) once is $O(md + nd^2)$, where $d = \max\{d_s | s \in \mathcal{S}\}$. In this way the complexity is on the same level as R-GCN [28], a commonly-used heterogeneous GNN variant, and it can be efficiently implemented through off-the-shelf sparse matrix libraries.

3.4 Generalization to Nonlinear Activations

In various message-passing GNNs [8, 14, 17, 28], node-wise ReLU activations are applied to the intermediate features during the forward propagation step. In our setting, by adding the additional regularization or constraints to our original energy function and using proximal gradient descent methods [23], the nonlinear activations can also be naturally derived without any heuristic modifications on our propagation step. Similar ideas have been applied to simpler homogeneous GNN models [34] More specifically, let $\phi_s : \mathbb{R}^{d_s} \rightarrow \mathbb{R}$ be an arbitrary convex function of node embeddings. Then, the optimization problem can be transformed into:

$$\ell_{\mathbf{Y}}(\mathbf{Y}) + \sum_{s \in \mathcal{S}} \sum_{i=1}^{n_s} \phi_s(\mathbf{y}_{si}). \quad (14)$$

Instead of directly minimizing (14) via vanilla gradient descent, we employ the proximal gradient descent (PGD) method [23] as follows. We first denote the relevant proximal operator as

$$\mathbf{prox}_{\phi}(\mathbf{v}) \triangleq \arg \min_{\mathbf{y}} \frac{1}{2} \|\mathbf{v} - \mathbf{y}\|_2^2 + \phi(\mathbf{y}). \quad (15)$$

Then, PGD iteratively minimizes (14) by computing

$$\bar{\mathbf{Y}}_s^{(k+1)} := \mathbf{Y}_s^{(k)} - \alpha \tilde{\mathbf{D}}_s^{-1} \nabla_{\mathbf{Y}_s^{(k)}} \ell_{\mathbf{Y}}(\mathbf{Y}) \quad (16)$$

$$\mathbf{Y}_s^{(k+1)} := \mathbf{prox}_{\phi_s}(\bar{\mathbf{Y}}_s^{(k+1)}). \quad (17)$$

For our purposes, we set $\phi_s(\mathbf{y}) \triangleq \sum_{i=1}^{d_s} \mathcal{I}_{\infty}[y_i < 0]$, in which \mathcal{I}_{∞} is an indicator function that assigns an infinite penalty to any $y_i < 0$, then, the corresponding proximal operator can be applied to each dimension independently and becomes $\mathbf{prox}_{\phi}(\mathbf{v}) = \text{ReLU}(\mathbf{v}) = \max(\mathbf{0}, \mathbf{v})$.

3.5 The Overall Algorithm

After performing K iterations of (25) with the proximal operator in (17), we obtain $\mathbf{Y}^{(K)}(\mathcal{W}, \mathcal{H})$, and the loss function for the downstream task becomes

$$\ell_{\mathcal{W}, \mathcal{H}}(\mathcal{W}, \mathcal{H}, \Theta) = \sum_{s \in \mathcal{S}'} \sum_{i=1}^{n'_s} \mathcal{D}(g_s[\mathbf{y}_{si}^{(K)}(\mathcal{W}, \mathcal{H}); \boldsymbol{\theta}_s], \mathbf{t}_{si}), \quad (18)$$

where \mathcal{S}' denotes a set of labeled node types, $g_s : \mathbb{R}^{d_s} \rightarrow \mathbb{R}^{c_s}$ denotes a node-wise function parameterized by $\boldsymbol{\theta}_s$, $\Theta \triangleq \{\boldsymbol{\theta}_s\}_{s \in \mathcal{S}'}$ denotes a set of parameters of g_s , and $\mathbf{t}_{si} \in \mathbb{R}^{c_s}$ is a ground-truth node-wise target⁵. Finally, we optimize (18) over \mathcal{W} and \mathcal{H} .

We dub the model obtained by above procedure as HALO (*Heterogeneous Architecture Leveraging Optimization*), and Algorithm 1 summarizes the overall process.

Algorithm 1 HALO algorithm

Require: \mathcal{G} : Heterogeneous graph dataset

Require: λ, α : Hyperparameters, K : Number of unfolding steps, E : Number of epochs

Randomly initialize $\mathbf{H}_t \in \mathcal{H}$, $\mathbf{W}_s \in \mathcal{W}$, and $\boldsymbol{\theta}_s \in \Theta$

for $e = 1, \dots, E$ **do**

Set $\mathbf{Y}_s^{(0)} = f(\mathbf{X}_s; \mathbf{W}_s)$ for all $s \in \mathcal{S}$

for $k = 0, \dots, K - 1$ **do**

Compute (16) (using (25)) and (17) to get $\mathbf{Y}_s^{(k+1)}$ for each $s \in \mathcal{S}$

end for

Compute $\ell_{\mathcal{W}, \mathcal{H}}(\mathcal{W}, \mathcal{H}, \Theta)$ using $\mathbf{Y}_s^{(K)}$

Update all $\mathbf{W}_s \in \mathcal{W}$, $\mathbf{H}_t \in \mathcal{H}$, and $\boldsymbol{\theta}_s \in \Theta$

end for

⁵Note that w.l.o.g., we assume that only the first $n'_s < n_s$ type- s nodes have labels for training.

Table 1: Results on HGB (left) and 4 knowledge graphs (right). The results are averaged over 5 runs.

| Model | DBLP | IMDB | ACM | Freebase | Avg. |
|----------------|--------------|--------------|--------------|--------------|--------------|
| R-GCN[28] | 92.07 | 62.05 | 91.41 | 58.33 | 75.97 |
| HAN[32] | 92.05 | 54.63 | 90.79 | 54.77 | 73.06 |
| HGT[11] | 93.49 | 67.20 | 91.00 | 60.51 | 78.05 |
| Simple-HGN[17] | 94.46 | 67.36 | 93.35 | 66.29 | 80.37 |
| HALO | 96.30 | 76.20 | 94.33 | 62.06 | 82.22 |

| Model | AIFB | MUTAG | BGS | AM | Avg. |
|-------------|--------------|--------------|--------------|--------------|--------------|
| Feat[25] | 55.55 | 77.94 | 72.41 | 66.66 | 68.14 |
| WL[29, 3] | 80.55 | 80.88 | 86.20 | 87.37 | 83.75 |
| RDF2Vec[27] | 88.88 | 67.20 | 87.24 | 88.33 | 82.91 |
| R-GCN[28] | 95.83 | 73.33 | 83.10 | 89.29 | 85.39 |
| HALO | 96.11 | 86.17 | 93.10 | 90.20 | 91.40 |

4 Experiments

We evaluate HALO on node or entity classification tasks from the heterogeneous graph benchmark (HGB) [17] and datasets consist of 4 knowledge graphs [28], and compare with state-of-the-art baselines. Furthermore, we also evaluate w.r.t. ZooBP under settings that permit direct comparisons, and we carry out further empirical analysis and ablations.

4.1 Node classification on benchmark datasets

The dataset descriptions are as follows:

HGB contains 4 node classification datasets, which is our focus herein. These include: DBLP, IMDB, ACM, and Freebase. DBLP and ACM are citation networks, IMDB is a movie information graph, and Freebase is a large knowledge graph. Except for Freebase, all datasets have node features. For more details, please refer to [17].

The **knowledge graph** benchmarking proposed in [28] is composed of 4 datasets: AIFB, MUTAG, BGS, AM. Using them, we classify the entities of target nodes. AIFB and MUTAG are relatively small scale knowledge graphs, and BGS and AM are large scale. Note that the AM dataset has more than 1M entities. For more details, please refer to [28].

In all experiments, we choose $f(\mathbf{X}_s; \mathbf{W}_s)$ and $g_s(\mathbf{y}_s, \boldsymbol{\theta}_s)$ as linear functions for all $s \in \mathcal{S}$, and when d_{s0} is different across the node types, $f(\mathbf{X}_s; \mathbf{W}_s)$ tries to match the dimension of each feature. All models and experiments were implemented using the PyTorch [24] and the Deep Graph Library (DGL) [31]. For the details on the hyperparameters and other experimental settings, please see the Supplementary Materials.

Table 1 shows the results on node classification tasks, where the best results are highlighted in bold. The left side of the table shows the results on HGB, and we report the results for [28], HAN [32], HGT [11], and Simple-HGN [17].⁶ The right side shows the results on knowledge graphs, where we report comparisons with R-GCN [28], hand-designed feature extractors (Feat) [25], Weisfeiler-Lehman kernels (WL), and RDF2Vec embeddings [27]. The Avg. column in each table represents the average of the results across the four datasets. In the table, HALO achieves the highest average accuracy, and outperforms the baselines on 7 of 8 datasets.

4.2 Comparison with ZooBP

We next compare HALO with ZooBP [5], which provided motivation for our use of compatibility matrices and represents a natural baseline to evaluate against when possible. ZooBP is a belief propagation method for heterogeneous graphs, and therefore the number of classes per node types should be pre-defined. Consequently, running ZooBP on HGB or the knowledge graph datasets in which only a single node type has labels is not feasible. Instead, to compare with ZooBP, we modified the DBLP and Academic [30] datasets so that all node types have labels. In both graphs, we removed ‘‘Term’’ and ‘‘Venue’’ types, and set the labels of ‘‘Paper’’ as the index of ‘‘Venue’’ nodes. As a result, the 20 and 18 Venues become labels on Papers in DBLP and Academic, respectively. Note that the Authors in both datasets have 4 classes, and since the DBLP has only two node types and two edge types, ‘‘Author-Paper’’ and ‘‘Paper-Author’’, it becomes a bipartite graph, and we call this ‘‘DBLP-bipartite’’. The Academic dataset has the edges between ‘‘Paper’’ node types, ‘‘Paper-cite-Paper’’, so it is not a bipartite graph. To ease the difficulty of node classification on Papers, we reduce the number of classes k of Papers to 4 based on their corresponding category. For choosing the fixed compatibility matrix for ZooBP (as a label propagation-like methods, ZooBP has no mechanism for training), when $k = 4$, we set $\mathbf{H}_t = \mathbf{I}_{k \times k} - \frac{1}{4} \mathbf{1}_{k \times k}$, where $\mathbf{1}_k$ is a $k \times k$ square matrix in which all

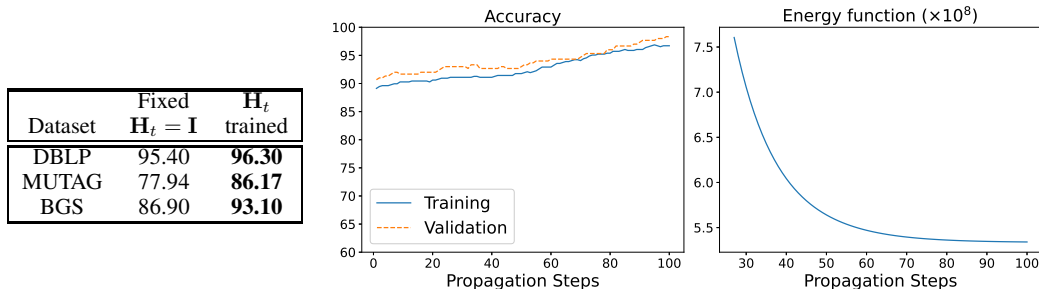
⁶To keep our work to be anonymous, we did not submit the results to HGB leaderboard [17], and we instead report the validation results.

Table 2: Comparison with ZooBP

| Dataset | DBLP-bipartite | | Academic | |
|--------------------|------------------------------|------------------------------|------------------------------|------------------------------|
| Node types | Author / Paper / All | | Author / Paper / All | |
| # Classes of Paper | $k = 4$ | $k = 20$ | $k = 4$ | $k = 18$ |
| ZooBP[5] | 63.00 / 63.60 / 63.47 | 62.00 / 19.53 / 28.47 | 79.63 / 73.43 / 75.97 | 81.76 / 16.08 / 42.94 |
| Ours | 76.50 / 64.13 / 66.79 | 78.50 / 33.33 / 43.00 | 96.63 / 93.89 / 94.93 | 97.81 / 84.73 / 90.18 |

elements are 1, and when $k = 18$ or $k = 20$, we set the matrix regarding the categories of each paper. In our case, we set $g_s(\mathbf{y}_s, \boldsymbol{\theta}_s)$ as identity, *i.e.*, $\boldsymbol{\theta}_s = \mathbf{I}$, and we treat \mathbf{y}_s as a score vector on each class. For further details on reducing the number of classes and choosing the compatibility matrix, please see the Supplementary Materials.

Table 2 shows the results of ZooBP and HALO in DBLP-bipartite and Academic datasets. We also report the classification accuracy on ‘‘Author’’ and ‘‘Paper’’ types. From these results, we observe that HALO outperforms ZooBP in all settings. For large k , the gap is more significant. The main reason for this phenomenon is that while HALO utilizes both node features and trainable compatibility matrices, ZooBP only uses training labels with fixed compatibility matrices. To the best of our knowledge, HALO is the only method designed to exploit a trainable compatibility matrix.

Table 3: Ablation study on \mathbf{H}_t Figure 1: Accuracy and energy function value versus the number of propagation steps on ACM.

4.3 Analysis

In this section, we carry out an ablation study on the compatibility matrix $\mathbf{H}_t \in \mathcal{H}$ by setting $\mathbf{H}_t = \mathbf{I}$, and show also show the accuracy and energy values of HALO versus the number of propagation steps.

Ablation study Table 3 shows the ablation study results. For this experiment, to set $\mathbf{H}_t = \mathbf{I}$, we used same embedding dimensions across all node types. Our method achieves higher accuracy than $\mathbf{H}_t = \mathbf{I}$ in all datasets. In DBLP, the margin between two methods relatively small, but in MUTAG and BGS, the accuracy gap is significant. These results show that using trainable compatibility matrix to address the mismatch between neighboring nodes is effective to perform a node classification tasks with heterogeneous graphs. Especially in MUTAG and BGS, we may infer that training \mathbf{H}_t can effectively capture the relation-dependent information. Note that while the embedding dimensions are same in this setting, there are still relation-specific mismatches between two different node types which have heterophily characteristic, and the trainable compatibility matrix can resolves this issue.

Results on propagation steps Figure 1 shows the results with various propagation steps. The left figure shows the training and validation accuracy on ACM dataset, and the right plot shows the energy function value (9) during the unfolding steps. In this figure, as we expected, when we increase the number of propagation steps with appropriate α , both training and validation accuracy are gradually increasing, and the energy function value steadily decreasing. This result indicates that the gradient descent steps gradually decreases the energy function, and this procedure produces node embeddings \mathbf{Y}_s that are useful for performing the downstream task.

5 Conclusion

In this paper, we have proposed HALO, a novel HGNN architecture derived from the minimization steps of a relation-aware energy function, the latter consisting of trainable relation-dependent compatibility matrices that can resolve the mismatch between two different node types. Because of

intrinsic properties of this unfolding framework, HALO is naturally robust to oversmoothing problems, and outperforms SOTA models on various benchmark datasets. For future work, extending HALO to spatio-temporal graphs in which the node and edge information change continuously can be considered.

References

- [1] Owe Axelsson. *Iterative solution methods*. Cambridge university press, 1996.
- [2] Jiuhai Chen, Jonas Mueller, Vassilis N Ioannidis, Soji Adeshina, Yangkun Wang, Tom Goldstein, and David Wipf. Does your graph need a confidence boost? convergent boosted smoothing on graphs with tabular node features. In *International Conference on Learning Representations*, 2021.
- [3] Gerben Klaas Dirk De Vries and Steven De Rooij. Substructure counting graph kernels for machine learning from rdf data. *Journal of Web Semantics*, 35:71–84, 2015.
- [4] Yuxiao Dong, Nitesh V Chawla, and Ananthram Swami. metapath2vec: Scalable representation learning for heterogeneous networks. In *Proceedings of the 23rd ACM SIGKDD international conference on knowledge discovery and data mining*, pages 135–144, 2017.
- [5] Dhivya Eswaran, Stephan Günnemann, Christos Faloutsos, Disha Makhija, and Mohit Kumar. Zoobp: Belief propagation for heterogeneous networks. *Proc. VLDB Endow.*, 10(5):625–636, jan 2017.
- [6] Xinyu Fu, Jiani Zhang, Ziqiao Meng, and Irwin King. Magnn: Metapath aggregated graph neural network for heterogeneous graph embedding. In *Proceedings of The Web Conference 2020*, pages 2331–2341, 2020.
- [7] Johannes Gasteiger, Aleksandar Bojchevski, and Stephan Günnemann. Combining neural networks with personalized pagerank for classification on graphs. In *International Conference on Learning Representations*, 2019.
- [8] Will Hamilton, Zhitaoying, and Jure Leskovec. Inductive representation learning on large graphs. *Advances in neural information processing systems*, 30, 2017.
- [9] Harold V. Henderson and S. R. Searle. The vec-permutation matrix, the vec operator and kronecker products: a review. *Linear and Multilinear Algebra*, 9(4):271–288, 1981.
- [10] Ziniu Hu, Yuxiao Dong, Kuansan Wang, Kai-Wei Chang, and Yizhou Sun. Gpt-gnn: Generative pre-training of graph neural networks. In *Proceedings of the 26th ACM SIGKDD International Conference on Knowledge Discovery & Data Mining*, pages 1857–1867, 2020.
- [11] Ziniu Hu, Yuxiao Dong, Kuansan Wang, and Yizhou Sun. Heterogeneous graph transformer. In *Proceedings of The Web Conference 2020*, pages 2704–2710, 2020.
- [12] Vassilis N Ioannidis, Meng Ma, Athanasios N Nikolakopoulos, Georgios B Giannakis, and Daniel Romero. Kernel-based inference of functions on graphs. In D. Comminiello and J. Principe, editors, *Adaptive Learning Methods for Nonlinear System Modeling*. Elsevier, 2018.
- [13] Diederick P Kingma and Jimmy Ba. Adam: A method for stochastic optimization. In *International Conference on Learning Representations (ICLR)*, 2015.
- [14] Thomas N Kipf and Max Welling. Semi-supervised classification with graph convolutional networks. 2017.
- [15] Guohao Li, Matthias Muller, Ali Thabet, and Bernard Ghanem. Deepgcns: Can gcns go as deep as cnns? In *Proceedings of the IEEE/CVF international conference on computer vision*, pages 9267–9276, 2019.
- [16] Qimai Li, Zhichao Han, and Xiao-ming Wu. Deeper insights into graph convolutional networks for semi-supervised learning. *Proceedings of the AAAI Conference on Artificial Intelligence*, 32, Apr. 2018.
- [17] Qingsong Lv, Ming Ding, Qiang Liu, Yuxiang Chen, Wenzheng Feng, Siming He, Chang Zhou, Jianguo Jiang, Yuxiao Dong, and Jie Tang. Are we really making much progress? revisiting, benchmarking and refining heterogeneous graph neural networks. In *Proceedings of the 27th ACM SIGKDD Conference on Knowledge Discovery & Data Mining, KDD '21*, page 1150–1160, New York, NY, USA, 2021. Association for Computing Machinery.

- [18] Yao Ma, Xiaorui Liu, Tong Zhao, Yozen Liu, Jiliang Tang, and Neil Shah. A unified view on graph neural networks as graph signal denoising. *arXiv preprint arXiv:2010.01777*, 2020.
- [19] Andrew L. Maas, Raymond E. Daly, Peter T. Pham, Dan Huang, Andrew Y. Ng, and Christopher Potts. Learning word vectors for sentiment analysis. In *Proceedings of the 49th Annual Meeting of the Association for Computational Linguistics: Human Language Technologies*, pages 142–150, Portland, Oregon, USA, June 2011. Association for Computational Linguistics.
- [20] Jorge Nocedal and Stephen J. Wright. *Numerical Optimization*. Springer, New York, NY, USA, 2e edition, 2006.
- [21] Kenta Oono and Taiji Suzuki. Graph neural networks exponentially lose expressive power for node classification. In *International Conference on Learning Representations*, 2020.
- [22] Xuran Pan, Shiji Song, and Gao Huang. A unified framework for convolution-based graph neural networks, 2021.
- [23] Neal Parikh, Stephen Boyd, et al. Proximal algorithms. *Foundations and Trends® in Optimization*, 1(3):127–239, 2014.
- [24] Adam Paszke, Sam Gross, Francisco Massa, Adam Lerer, James Bradbury, Gregory Chanan, Trevor Killeen, Zeming Lin, Natalia Gimelshein, Luca Antiga, Alban Desmaison, Andreas Kopf, Edward Yang, Zachary DeVito, Martin Raison, Alykhan Tejani, Sasank Chilamkurthy, Benoit Steiner, Lu Fang, Junjie Bai, and Soumith Chintala. Pytorch: An imperative style, high-performance deep learning library. In H. Wallach, H. Larochelle, A. Beygelzimer, F. d'Alché-Buc, E. Fox, and R. Garnett, editors, *Advances in Neural Information Processing Systems 32*, pages 8024–8035. Curran Associates, Inc., 2019.
- [25] Heiko Paulheim and Johannes Fümkrantz. Unsupervised generation of data mining features from linked open data. In *Proceedings of the 2nd international conference on web intelligence, mining and semantics*, pages 1–12, 2012.
- [26] Judea Pearl. Reverend bayes on inference engines: A distributed hierarchical approach. In *Probabilistic and Causal Inference: The Works of Judea Pearl*, pages 129–138, 2022.
- [27] Petar Ristoski and Heiko Paulheim. Rdf2vec: Rdf graph embeddings for data mining. In *International Semantic Web Conference*, pages 498–514. Springer, 2016.
- [28] Michael Schlichtkrull, Thomas N Kipf, Peter Bloem, Rianne van den Berg, Ivan Titov, and Max Welling. Modeling relational data with graph convolutional networks. In *European semantic web conference*, pages 593–607. Springer, 2018.
- [29] Nino Shervashidze, Pascal Schweitzer, Erik Jan Van Leeuwen, Kurt Mehlhorn, and Karsten M Borgwardt. Weisfeiler-lehman graph kernels. *Journal of Machine Learning Research*, 12(9), 2011.
- [30] Jie Tang, Jing Zhang, Limin Yao, Juanzi Li, Li Zhang, and Zhong Su. Arnetminer: extraction and mining of academic social networks. In *Proceedings of the 14th ACM SIGKDD international conference on Knowledge discovery and data mining*, pages 990–998, 2008.
- [31] Minjie Wang, Da Zheng, Zihao Ye, Quan Gan, Mufei Li, Xiang Song, Jinjing Zhou, Chao Ma, Lingfan Yu, Yu Gai, Tianjun Xiao, Tong He, George Karypis, Jinyang Li, and Zheng Zhang. Deep graph library: A graph-centric, highly-performant package for graph neural networks. *arXiv preprint arXiv:1909.01315*, 2019.
- [32] Xiao Wang, Houye Ji, Chuan Shi, Bai Wang, Yanfang Ye, Peng Cui, and Philip S Yu. Heterogeneous graph attention network. In *The world wide web conference*, pages 2022–2032, 2019.
- [33] Yuto Yamaguchi, Christos Faloutsos, and Hiroyuki Kitagawa. Camlp: Confidence-aware modulated label propagation. pages 513–521. Proceedings of the 2016 SIAM International Conference on Data Mining (SDM), 2016.
- [34] Yongyi Yang, Tang Liu, Yangkun Wang, Jinjing Zhou, Quan Gan, Zhewei Wei, Zheng Zhang, Zengfeng Huang, and David Wipf. Graph neural networks inspired by classical iterative algorithms. In *International Conference on Machine Learning*, pages 11773–11783. PMLR, 2021.
- [35] Hongwei Zhang, Tijin Yan, Zenjun Xie, Yuanqing Xia, and Yuan Zhang. Revisiting graph convolutional network on semi-supervised node classification from an optimization perspective. *CoRR*, abs/2009.11469, 2020.

- [36] Dengyong Zhou, Olivier Bousquet, Thomas Lal, Jason Weston, and Bernhard Schölkopf. Learning with local and global consistency. In S. Thrun, L. Saul, and B. Schölkopf, editors, *Advances in Neural Information Processing Systems*, volume 16. MIT Press, 2003.
- [37] Meiqi Zhu, Xiao Wang, Chuan Shi, Houye Ji, and Peng Cui. Interpreting and unifying graph neural networks with an optimization framework. *arXiv preprint arXiv:2101.11859*, 2021.

6 Proof of Lemma 3.1

Before proceeding the proof of Lemma 3.1, we first provide basic mathematical results.

Lemma 6.1. (Roth's column lemma [9]). For any three matrices \mathbf{X} , \mathbf{Y} and \mathbf{Z} ,

$$\text{vec}(\mathbf{X}\mathbf{Y}\mathbf{Z}) = (\mathbf{Z}^\top \otimes \mathbf{X})\text{vec}(\mathbf{Y}) \quad (19)$$

Now, we begin the proof.

Proof. The gradient of (9, Manuscript) is as follows:

$$\nabla_{\mathbf{Y}_s} \ell_{\mathbf{Y}}(\mathbf{Y}) = (\mathbf{I} + \lambda \mathbf{D}_s) \mathbf{Y}_s - f(\mathbf{X}_s; \mathbf{W}_s) + \lambda \sum_{s' \in \mathcal{S}} \sum_{t \in \mathcal{T}_{ss'}} (\mathbf{D}_{st} \mathbf{Y}_s (\mathbf{H}_t \mathbf{H}_t^\top) - \mathbf{A}_t \mathbf{Y}_{s'} (\mathbf{H}_t^\top + \mathbf{H}_{t_{\text{inv}}})) \quad (20)$$

By taking $\text{vec}(\cdot)$ operation on both side of (20), (20) is changed to:

$$\begin{aligned} \text{vec}(\nabla_{\mathbf{Y}_s} \ell_{\mathbf{Y}}(\mathbf{Y})) &= \text{vec}(\mathbf{Y}_s) - \text{vec}(f(\mathbf{X}_s; \mathbf{W}_s)) \\ &+ \lambda \left(\sum_{s' \in \mathcal{S}} \sum_{t \in \mathcal{T}_{ss'}} (\text{vec}(\mathbf{D}_{st} \mathbf{Y}_s (\mathbf{H}_t \mathbf{H}_t^\top)) - \text{vec}(\mathbf{A}_t \mathbf{Y}_{s'} (\mathbf{H}_t^\top + \mathbf{H}_{t_{\text{inv}}})) \right) + \text{vec}(\mathbf{D}_s \mathbf{Y}_s) \end{aligned} \quad (21)$$

Here, using Roth's column lemma 6.1, we define the matrix \mathbf{P} , \mathbf{Q} , \mathbf{R} as follows:

$$\begin{aligned} \mathbf{P} &= \begin{bmatrix} \mathbf{P}_{11} & \dots & \mathbf{P}_{1|S|} \\ \dots & \dots & \dots \\ \mathbf{P}_{|S|1} & \dots & \mathbf{P}_{|S||S|} \end{bmatrix}; \mathbf{P}_{ss'} = \sum_{t \in \mathcal{T}_{ss'}} ((\mathbf{H}_t^\top + \mathbf{H}_{t_{\text{inv}}}) \otimes \mathbf{A}_t) \\ \mathbf{Q} &= \bigoplus_{s \in \mathcal{S}} \mathbf{Q}_s; \mathbf{Q}_s = \sum_{s' \in \mathcal{S}} \sum_{t \in \mathcal{T}_{ss'}} (\mathbf{H}_t \mathbf{H}_t^\top \otimes \mathbf{D}_{st}), \mathbf{D} = \bigoplus_{s \in \mathcal{S}} \mathbf{I} \otimes \mathbf{D}_s. \end{aligned}$$

Therefore, we can rewrite (21) as:

$$\begin{aligned} \text{vec}(\nabla_{\mathbf{Y}_s} \ell_{\mathbf{Y}}(\mathbf{Y})) &= \text{vec}(\mathbf{Y}_s) - \text{vec}(f(\mathbf{X}_s; \mathbf{W}_s)) \\ &+ \lambda (\mathbf{Q}_s \text{vec}(\mathbf{Y}_s) - \sum_{s' \in \mathcal{S}} \mathbf{P}_{ss'} \text{vec}(\mathbf{Y}_{s'}) + \mathbf{D}_s \text{vec}(\mathbf{Y}_s)) \end{aligned} \quad (22)$$

Stacking $|S|$ such matrix equations together and rewriting using \mathbf{P} , \mathbf{Q} , \mathbf{D} , (22) can be written as:

$$\text{vec}(\nabla_{\mathbf{Y}} \ell_{\mathbf{Y}}(\mathbf{Y})) = \text{vec}(\mathbf{Y}) - \text{vec}(\tilde{f}(\tilde{\mathbf{X}}; \mathcal{W})) + \lambda (\mathbf{Q} - \mathbf{P} + \mathbf{D}) \text{vec}(\mathbf{Y}) \quad (23)$$

Since $\ell_{\mathbf{Y}}(\mathbf{Y})$ is a convex function, a point that achieves $\nabla_{\mathbf{Y}} \ell_{\mathbf{Y}}(\mathbf{Y}) = 0$ is a optimal point. Therefore, the closed-form solution for $\text{vec}(\mathbf{Y}^*(\mathcal{W}, \mathcal{H}))$ is derived as:

$$\text{vec}(\mathbf{Y}^*(\mathcal{W}, \mathcal{H})) = (\mathbf{I} + \lambda (\mathbf{Q} - \mathbf{P} + \mathbf{D}))^{-1} \text{vec}(\tilde{f}(\tilde{\mathbf{X}}; \mathcal{W})) \quad (24)$$

□

7 Proof of Theorem 3.2

Proof. The iteration $k + 1$ of gradient descent on \mathbf{Y}_s with preconditioning is as follows:

$$\mathbf{Y}_s^{(k+1)} = \mathbf{Y}_s^{(k)} - \alpha \tilde{\mathbf{D}}_s^{-1} \nabla_{\mathbf{Y}_s^{(k)}} \ell_{\mathbf{Y}}(\mathbf{Y}) \quad (25)$$

By applying $\text{vec}(\cdot)$ operation to both side of 25, this can be transformed into:

$$\text{vec}(\mathbf{Y}_s^{(k+1)}) = \text{vec}(\mathbf{Y}_s^{(k)}) - \alpha \text{vec}(\tilde{\mathbf{D}}_s^{-1} \nabla_{\mathbf{Y}_s^{(k)}} \ell_{\mathbf{Y}}(\mathbf{Y})) \quad (26)$$

$$= \text{vec}(\mathbf{Y}_s^{(k)}) - \alpha (\mathbf{I} \otimes \tilde{\mathbf{D}}_s^{-1}) \text{vec}(\nabla_{\mathbf{Y}_s^{(k)}} \ell_{\mathbf{Y}}(\mathbf{Y})) \quad (27)$$

Note that we apply Roth's column lemma to (26) to derive (27). Stacking $|S|$ such vectors together, (27) can be written as:

$$\text{vec}(\mathbf{Y}^{(k+1)}) = \text{vec}(\mathbf{Y}^{(k)}) - \alpha \tilde{\mathbf{D}}^{-1} \text{vec}(\nabla_{\mathbf{Y}^{(k)}} \ell_{\mathbf{Y}}(\mathbf{Y})), \quad (28)$$

where $\tilde{\mathbf{D}}^{-1} \triangleq \bigoplus_{s \in \mathcal{S}} \mathbf{I} \otimes \tilde{\mathbf{D}}_s^{-1}$.

In convex function, there exists $\mathbf{Y}^{(k+1)}$ and $\mathbf{Y}^{(k)}$ that such that the following inequality holds:

$$\begin{aligned} \ell_{\mathbf{Y}}(\mathbf{Y}^{(k+1)}) &\leq \ell_{\mathbf{Y}}(\mathbf{Y}^{(k)}) + \text{vec}(\nabla_{\mathbf{Y}^{(k)}} \ell_{\mathbf{Y}}(\mathbf{Y}))^\top \text{vec}(\mathbf{Y}^{(k+1)} - \mathbf{Y}^{(k)}) \\ &\quad + \frac{1}{2} \text{vec}(\mathbf{Y}^{(k+1)} - \mathbf{Y}^{(k)})^\top \nabla^2 \ell_{\mathbf{Y}^{(k)}}(\mathbf{Y}) \text{vec}(\mathbf{Y}^{(k+1)} - \mathbf{Y}^{(k)}), \end{aligned} \quad (29)$$

where $\nabla_{\mathbf{Y}^{(k)}}^2 \ell_{\mathbf{Y}}(\mathbf{Y})$ is a Hessian matrix whose elements are $\nabla_{\mathbf{Y}^{(k)}}^2 \ell_{\mathbf{Y}}(\mathbf{Y})_{ij} = \frac{\partial^2 \ell_{\mathbf{Y}}(\mathbf{Y})}{\partial \text{vec}(\mathbf{Y})_i \partial \text{vec}(\mathbf{Y})_j} \Big|_{\mathbf{Y}=\mathbf{Y}^{(k)}}$.

Plugging in the gradient descent update by letting $\text{vec}(\mathbf{Y}^{(k+1)} - \mathbf{Y}^{(k)}) = -\alpha \tilde{\mathbf{D}}^{-1} \text{vec}(\nabla_{\mathbf{Y}^{(k)}} \ell_{\mathbf{Y}}(\mathbf{Y}))$, we get:

$$\begin{aligned} \ell(\mathbf{Y}^{(k+1)}) &\leq \ell(\mathbf{Y}^{(k)}) - (\tilde{\mathbf{D}}^{-1} \text{vec}(\nabla_{\mathbf{Y}^{(k)}} \ell_{\mathbf{Y}}(\mathbf{Y})))^\top (\alpha \tilde{\mathbf{D}}) (\tilde{\mathbf{D}}^{-1} \text{vec}(\nabla_{\mathbf{Y}^{(k)}} \ell_{\mathbf{Y}}(\mathbf{Y}))) \\ &\quad + (\tilde{\mathbf{D}}^{-1} \text{vec}(\nabla_{\mathbf{Y}^{(k)}} \ell_{\mathbf{Y}}(\mathbf{Y})))^\top \left(\frac{\alpha^2}{2} \nabla^2 \ell_{\mathbf{Y}^{(k)}}(\mathbf{Y}) \right) (\tilde{\mathbf{D}}^{-1} \text{vec}(\nabla_{\mathbf{Y}^{(k)}} \ell_{\mathbf{Y}}(\mathbf{Y}))) \end{aligned} \quad (30)$$

If $\alpha \tilde{\mathbf{D}} - \frac{\alpha^2}{2} \nabla_{\mathbf{Y}^{(k)}}^2 \ell_{\mathbf{Y}}(\mathbf{Y}) \succ 0$ holds, then gradient descent can always decrease the loss. To compute $\nabla_{\mathbf{Y}^{(k)}}^2 \ell_{\mathbf{Y}}(\mathbf{Y})$, we differentiate (23), and we get:

$$\nabla_{\mathbf{Y}^{(k)}}^2 \ell_{\mathbf{Y}}(\mathbf{Y}) = \mathbf{I} + \lambda(\mathbf{Q} - \mathbf{P} + \mathbf{D}) \quad (31)$$

Going back to the above inequality, we can proceed the following:

$$\begin{aligned} \alpha \tilde{\mathbf{D}} - \frac{\alpha^2}{2} (\mathbf{I} + \lambda(\mathbf{Q} - \mathbf{P} + \mathbf{D})) &= \alpha (\mathbf{I} + \lambda \mathbf{D}) - \frac{\alpha^2}{2} (\mathbf{I} + \lambda(\mathbf{Q} - \mathbf{P} + \mathbf{D})) \\ &= \left(\alpha - \frac{\alpha^2}{2} \right) (\mathbf{I} + \lambda \mathbf{D}) - \frac{\alpha^2 \lambda}{2} (\mathbf{Q} - \mathbf{P}) \\ &\succ \left(\alpha - \frac{\alpha^2}{2} \right) (1 + \lambda d_{\min}) \mathbf{I} - \frac{\alpha^2 \lambda}{2} (\mathbf{Q} - \mathbf{P}), \end{aligned} \quad (32)$$

where $d_{\min} \triangleq \min_i \mathbf{D}_{ii}$. If α satisfies $\left(\alpha - \frac{\alpha^2}{2} \right) (1 + \lambda d_{\min}) \mathbf{I} - \frac{\alpha^2 \lambda}{2} (\mathbf{Q} - \mathbf{P}) \succ 0$, then $\alpha \tilde{\mathbf{D}} - \frac{\alpha^2}{2} \nabla_{\mathbf{Y}^{(k)}}^2 \ell_{\mathbf{Y}}(\mathbf{Y}) \succ 0$ holds. Therefore, the sufficient condition for the convergence is:

$$\left(\alpha - \frac{\alpha^2}{2} \right) (1 + \lambda d_{\min}) - \frac{\alpha^2 \lambda}{2} \sigma_{\max} > 0, \quad (33)$$

where σ_{\max} is a maximum eigenvalue of $(\mathbf{Q} - \mathbf{P})$. As a result, we get the following inequality:

$$\alpha < \frac{2 + 2\lambda d_{\min}}{1 + \lambda(d_{\min} + \sigma_{\max})} \quad (34)$$

□

8 Details on Experiment Settings

8.1 Hyperparameters

In the all experiments, we used Adam optimizer [13] and used dropout as regularization with dropout rate 0.5. For other hyperparameters, please refer to Table 4.

Table 4: Model Hyperparameters for HALO

| Datasets | DBLP | IMDB | ACM | Freebase | AIFB | MUTAG | BGS | AM |
|-------------------|-----------|-----------|-----------|-----------|-----------|-----------|-----------|-----------|
| Hidden Layer Size | 256 | 64 | 32 | 32 | 16 | 16 | 16 | 16 |
| Learning Rate | 10^{-4} | 10^{-3} | 10^{-2} | 10^{-2} | 10^{-3} | 10^{-3} | 10^{-2} | 10^{-2} |
| Weight Decay | 10^{-5} | 10^{-5} | 10^{-4} | 10^{-3} | 10^{-5} | 10^{-4} | 10^{-5} | 10^{-4} |
| K | 8 | 32 | 32 | 4 | 16 | 16 | 8 | 4 |
| λ | 1 | 1 | 0.1 | 1 | 1 | 0.01 | 0.1 | 1 |
| α | 1 | 1 | 0.1 | 1 | 0.1 | 1 | 1 | 1 |

8.2 Categorization in DBLP and Academic datasets

To carry out experiments for ZooBP, we modified DBLP and Academic datasets. Here, we give details on categorization of venues in DBLP and Academic datasets. Each venue is the name of academic conference.

DBLP dataset has 20 venues: AAAI, CVPR, ECML, ICML, IJCAI, SIGMOD, VLDB, EDBT, ICDE, PODS, ICDM, KDD, PAKDD, PKDD, SDM, CIKM, CIR, SIGIR, WSDM, WWW. We categorize the above venues to 4 categories: **ML** (AAAI, CVPR, ECML, ICML, IJCAI), **DB** (SIGMOD, VLDB, EDBT, ICDE, PODS), **DM** (ICDM, KDD, PAKDD, PKDD, SDM), and **IR**(CIKM, CIR, SIGIR, WSDM, WWW).

Academic dataset has 18 venues: ICML, AAAI, IJCAI, CVPR, ICCV, ECCV, ACL, EMNLP, NAACL, KDD, WSDM, ICDM, SIGMOD, VLDB, ICDE, WWW, SIGIR, CIKM. We categorize the above venues to 4 categories: **ML** (ICML, AAAI, IJCAI), **Vision** (CVPR, ICCV, ECCV), **NLP** (ACL, EMNLP, NAACL), and **Data** (KDD, WSDM, ICDM, SIGMOD, VLDB, ICDE, WWW< SIGIR, CIKM).

For choosing the compatibility matrix of ZooBP, based on the statistics of each dataset, if the class i for “Paper” and the class j for “Author” is highly correlated, we give high positive value on $H(i, j)$ and $H(j, i)$. Otherwise, we give negative value to satisfy the residual condition of the compatibility matrix.